Pergamon

PII: S0191-8141(98)00035-2

Journal of Structural Geology, Vol. 20, No. 8, pp. 1089 to 1103, 1998

0191-8141/98 $19.00 + 0.00

Distinction between tectonic mixing and mass transfer processes in a ductile shear zone

X.-Y. YANG, K. D. O'HARA and D. P. MOECHER

Department of Geological Sciences, University of Kentucky, Lexington, KY 40506-0053, U.S.A.
E-mail: geokoh@pop.uky.ed

(*Received* 15 *October* 1996; *accepted in revised form* 26 *March* 1998)

Abstract—A petrological, geochemical and microtextural study of an upper amphibolite facies shear zone, developed in interlayered mafic and felsic layers, permits the relative roles of tectonic mixing and fluid-assisted mass transfer processes to be determined. Geochemical evidence indicates that the chemical changes in the deformed rocks result from mixing of mafic and felsic layers together with fluid-assisted mass transfer within the shear zone. During mylonitization, most major elements and some trace elements (LREE, Rb, Sr, Ba, Cu, Ni) exhibited mobile behavior. The HREEs, Ti, V, Sc, Co and Fe, on the other hand, were immobile. Based on mass conservation of these elements, a two-component mixing model using mafic and felsic rocks from outside the shear zone as end-members explains the major and trace element data. The chemical composition of the felsic mylonite is modeled by mixing $12 \pm 5\%$ mafic rock and $88 \pm 5\%$ felsic rock, whereas, the mafic mylonite is modeled by mixing $55 \pm 4\%$ mafic rock and $45 \pm 4\%$ felsic rock. A closed system mixing model yields a good fit for immobile elements, such as HREEs, Ti, V, and Sc, but significant chemical differences between the calculated data and observed data are explained by fluid-assisted mass transfer of mobile elements under open system conditions. A 24% volume loss in the felsic mylonite and 13% volume loss in mafic mylonite are derived from the mass balance, assuming the HREE, Ti, V and Sc were immobile.

INTRODUCTION

The formation and evolution of crustal shear zones commonly involve the interaction of mechanical, chemical, hydrological, and thermal processes resulting in production of distinctive features in mylonites and cataclasites such as grain-size reduction (by either crystal–plastic or brittle mechanisms), hydrous retrograde alteration (Beach, 1980; Janecke and Evans, 1988; Hickman *et al*., 1995) and volume changes related to fluid-assisted mass transfer (O'Hara, 1988; Glazner and Bartley, 1991; Goddard and Evans, 1995). An additional process in shear zones which can result in large chemical changes of the sheared rocks relative to the protolith rock, without necessarily involving fluids, is tectonic mixing. Tectonic mixing is recognized as an important low-temperature process in melanges (Rast and Horton, 1989) and brittle faults (Evans and Chester, 1995), and commonly involves at least two lithologies of contrasting strength. At higher metamorphic grades, where crystal–plastic mechanisms dominate, mixing may also be an important tectonic process. The highly strained banded gneisses in high grade metamorphic terranes, thought to be characteristic of the lower continental crust, are commonly the result of tectonic mixing of mafic and felsic components coupled with metamorphic reaction and partial melting during high grade shearing (Passchier *et al*., 1990). This paper presents a geochemical approach to distinguish between mixing and mass transfer processes in an upper amphibolite facies shear zone in the Parry Sound domain of the Grenville Province, Ontario, Canada. Modeling of major and trace element concentrations suggests that two-component mixing occurred between felsic and mafic rocks together with fluid-assisted mass transfer under open system conditions.

GEOLOGICAL SETTING AND OUTCROP DESCRIPTION

The Parry Sound shear zone (PSSZ) has been recognized as an 1–3 km wide ductile shear zone that separates the Parry Sound and Britt domains (Davidson *et al*., 1982) (Fig. 1), and it is characterized by highly flattened rocks with extreme grain-size reduction and mylonitic foliation. The domains are interpreted to represent large-scale slices of deep level crust, bounded by kilometer-wide zones of high strain and ductile shearing (Davidson, 1984). Kinematic indicators (such as rotated garnet and asymmetric feldspar porphyroclasts) in mafic and granitic gneisses indicate thrusting to the northwest along the PSSZ during the Grenville orogeny (Davidson, 1984; White and Mawer, 1986).

U–Pb dating of zircon and baddeleyite indicates that the peak of metamorphism in the Parry Sound domain occurred at 1160 Ma (van Breeman *et al*., 1986), in good agreement with a U–Pb monazite age of 1159 Ma (Tucillo *et al*., 1992). U–Pb isotopic ages of zircons from both highly and weakly deformed pegmatite dykes in the PSSZ yield 1159 Ma and 1121 Ma, respectively (van Breeman *et al*., 1986); this indicates that ductile shearing along the PSSZ took place during

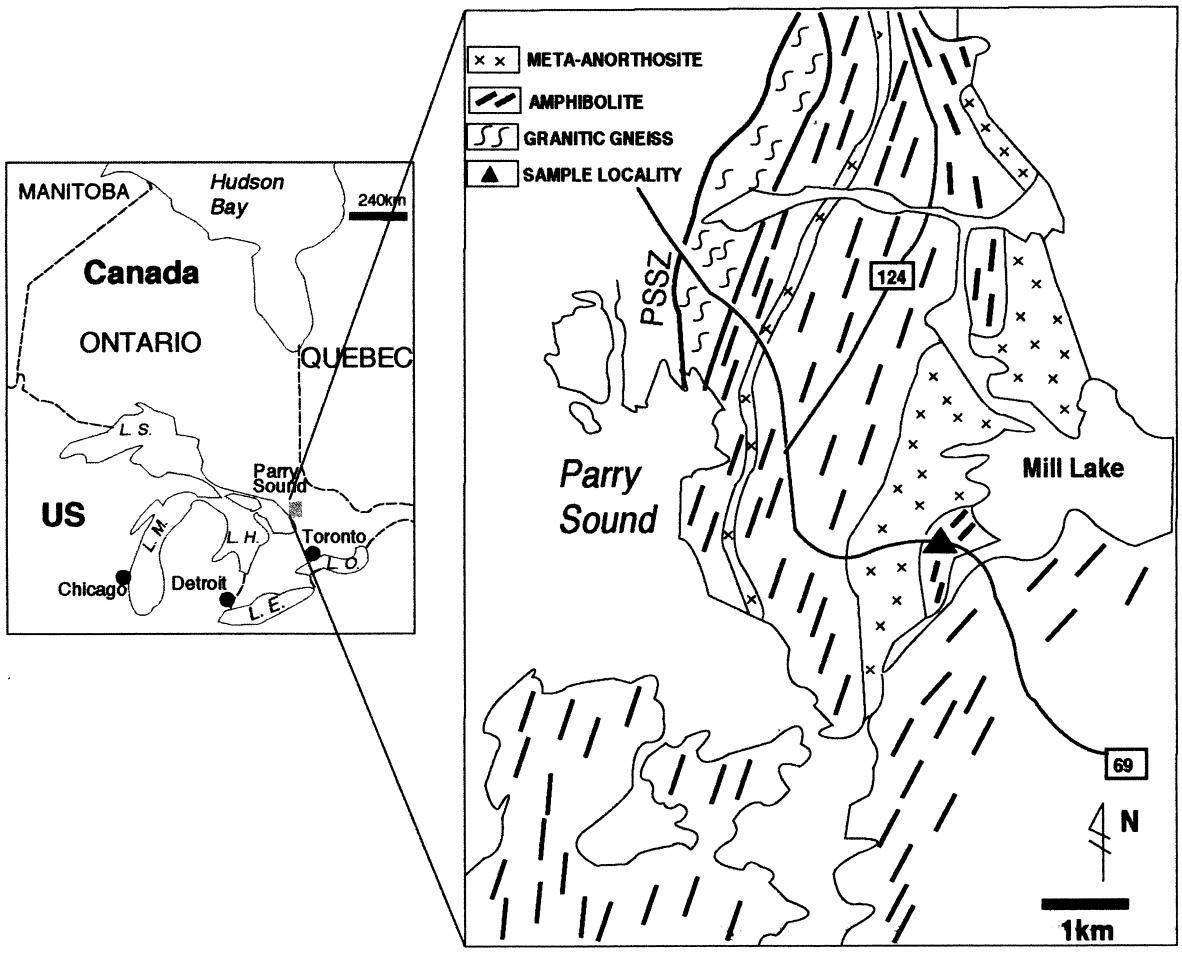

Fig. 1. General geological map of area within the vicinity of Parry Sound, Ontario, and the Parry Sound shear zone (PSSZ) (after Davidson, 1984; Moecher *et al.*, 1992). The locality of the studied normal shear zone (triangle) is at the junction of Ontario Highway 69 and Parry Sound Drive (old Highway 69).

and shortly after the peak of metamorphism. During thrusting, metamorphic pressures and temperatures reached 10 ± 1 kbar and $800 \pm 50°C$ (Anovitz and Essene, 1990; Moecher *et al.*, 1992). A post-thrusting extensional event was interpreted to result in an isobaric cooling path from 800°C to 600°C in the Parry Sound area (Anovitz and Chase, 1990). During extension, some granulite facies rocks were retrograded to amphibolite facies at a temperature of $600 \pm 50°C$ (Anovitz and Chase, 1990).

This study examines an outcrop-scale amphibolite grade normal shear zone within interlayered mafic and felsic layers (Fig. 2), located east of the Whitestone Anorthosite in the Parry Sound domain (Fig. 1). The shear zone is about 10 cm wide and dips southeastward at 56° (Fig. 2). It is interpreted to be associated with the extensional event noted above. A mafic layer in the hanging wall and a felsic layer in the footwall were sampled (Fig. 2b). The sampled mafic and felsic layers are about 10–15 cm thick outside the shear zone, but show a progressive decrease in thickness to 3–4 cm with increasing deformation within the shear zone (Fig. 2). The rocks between the two sampled layers consist of repetitious thin mafic and felsic layers which are the same lithologies as the sampled mafic and felsic layers (Fig. 2). The vertical displacement of the mafic layer (approximately 35 cm) is less than that of the felsic layer (about 60 cm), indicating that strain was heterogeneous on the outcrop scale. In this study, the least deformed samples (PS50 and PS80), which are also farthest from the shear zone (Fig. 2b), are treated as the protoliths of the mafic and felsic mylonites, respectively.

ANALYTICAL METHODS

Samples of mafic and felsic lithologies were trimmed of any adhering adjacent felsic and mafic layers, respectively. Rock samples (> 1 kg) were crushed to 200 mesh in a hardened steel shatter box, and after thorough mixing, an aliquot was taken for analysis. Whole rock mafic and felsic samples were analyzed for concentrations of major, trace, and rare earth elements (REE) and also $\delta^{18}O$ values. Major elements were determined twice in all samples by X-ray fluorescence (XRF) in two separate laboratories—at the Kentucky Geological Survey and commercially by XRAL

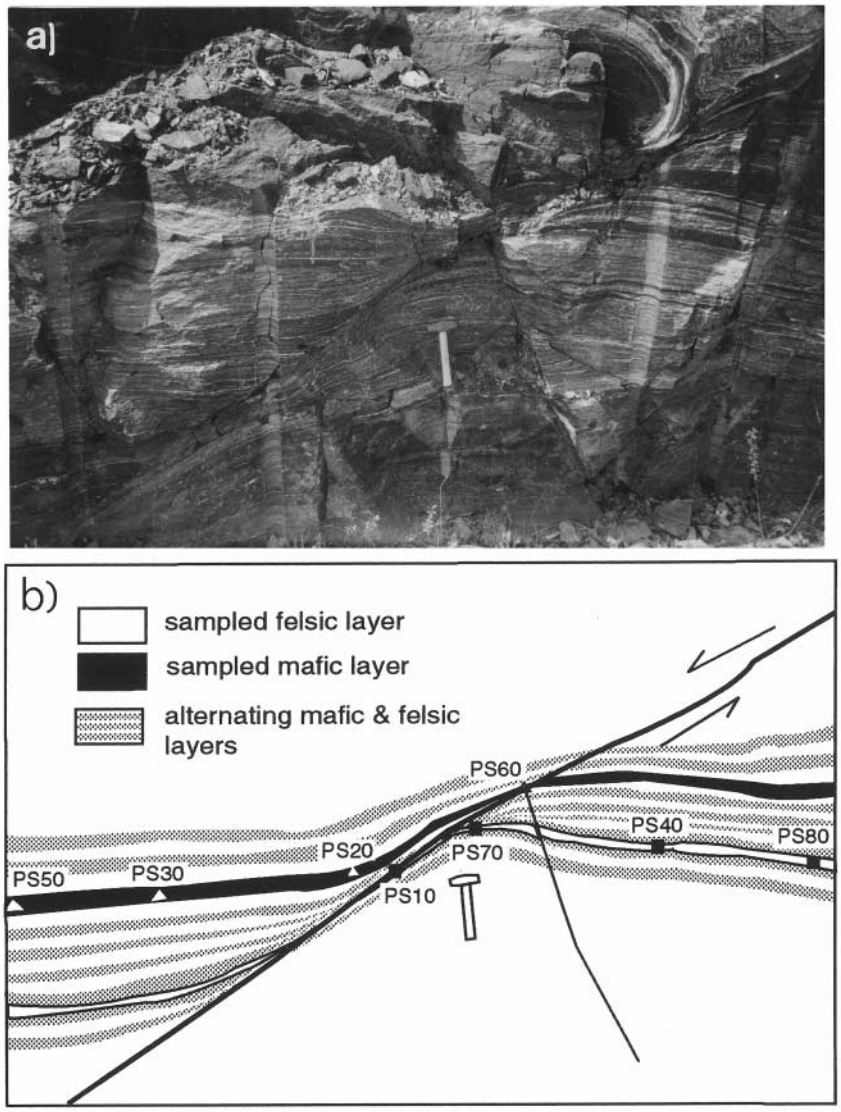

Fig. 2. (a) Field photograph of the normal shear zone. (b) Sample localities in the felsic and mafic layers. Note that the rocks between the sampled layers are interlayered felsic and mafic layers which are the same lithology as the sampled layers. The hammer handle is 35 cm long.

Activation Services, Inc. Interlaboratory comparison of the major element analyses indicates an absolute accuracy of better than 2% for Al, Si, Ca, Mg and 0.5% for other major elements. Replicate analyses of standards in both laboratories indicate a relative precision range (SD/mean) of less than 0.5% for most major elements. All trace elements of all samples were commercially analyzed by XRAL Activation Services, Inc. Zirconium, Y, and Rb were analyzed by XRF. Rare earth elements, U, Th, Hf, and Sc were determined by instrumental neutron activation analysis (INAA) and vanadium and other trace elements were determined by inductively coupled plasma (ICP). The standard deviation (1σ) for each element is determined through the replicate analyses of standards. Mineral compositions were analyzed by wavelength-dispersive analysis using an accelerating voltage of 15 kV, a beam current of 15 nA, and USNM mineral standards at the University of Kentucky electron microprobe facility. Whole rock oxygen isotope determinations were carried out at the University of Michigan using standard techniques and reported as $\delta^{18}O$ values relative to SMOW. Thin-sections were examined under a petrographic microscope and modal analyses were performed by using an electronic point counter ($n = 500$). Sample densities were obtained by measuring specific gravity on a balance and are accurate to 0.01 g/cc.

PETROLOGY AND MICROSTRUCTURE

Mafic layer

The mafic layer is characterized by repetitious mafic (hornblende) and felsic (plagioclase and quartz) rich bands which define the foliation. It consists of hornblende (51%–60%), plagioclase (27%–38%), quartz (2%–8%), and garnet (1%–13%) (Table 1).

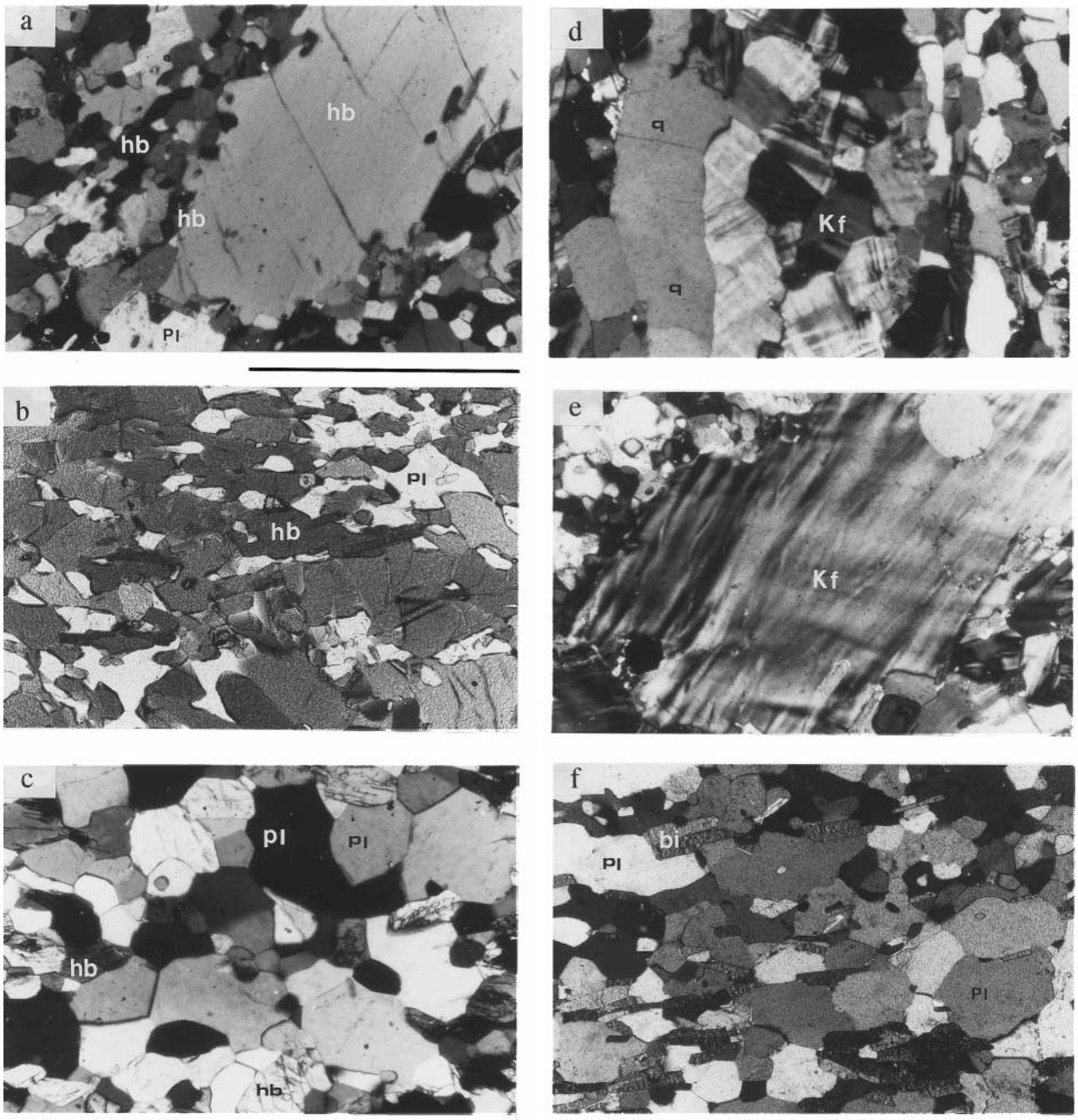

Fig. 3. Photomicrographs of the mafic (a–c) and felsic (d–f) samples. Scale bar is 1 mm. (a) Elongated hornblende (hb) porphyroblast in mafic protolith (sample PS50) showing undulatory extinction and recrystallized margins. (b) Recrystallized hornblende grains (hb) and andesine (pl) with straight boundaries and high angle contacts in mafic sample PS30. (c) Totally recrystallized equant andesine (pl) and hornblende (hb) grains showing foam texture in mafic mylonite (PS60). (d) Monocrystalline quartz (q) ribbon and recrystallized microcline (Kf) in felsic protolith (PS80). (e) Perthitic alkali feldspar (Kf) porphyroclast with recrystallized margins consisting of oligoclase and quartz in felsic protolith (PS80). (f) Totally recrystallized felsic mylonite consisting of oligoclase, quartz and biotite (bi).

Hornblende is present as two texturally distinct, but compositionally similar, varieties (Table 2)—coarse-grained porphyroblasts (0.3–1.0 mm) and finer recrystallized grains (40–120 μm; Fig. 3a & b). The coarse hornblende shows conspicuous lenticular monocrystalline grain shapes with aspect ratios of between 2:1 and 4:1 and a dimensional preferred orientation parallel to the foliation (Fig. 3a). They also display ubiquitous sweeping undulatory extinction and serrated grain boundaries. Fine-grained hornblende grains have straight grain boundaries and display slightly elongated shapes (Fig. 3b & c). The abundance of fine-grained recrystallized hornblende increases progressively toward the shear zone (Fig. 4), indicating grain-size reduction of hornblende with progressive deformation. Relict clino- and orthopyroxene are variably retrograded to hornblende, and garnet is pseudomorphed by recrystallized plagioclase grains, indicated by reaction rims around garnet porphyroblasts.

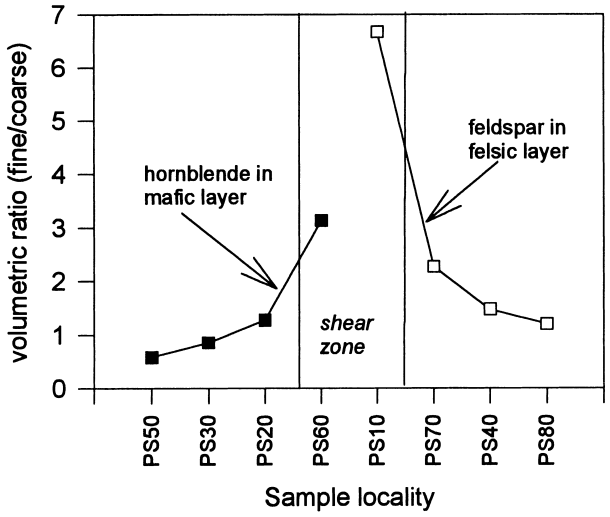

Fig. 4. Changes in ratio of fine-grained recrystallized grains to coarse-grained porphyroblasts of hornblende and feldspar as a function of distance to the shear zone. Based on counting of 500 points per sample.

Two generations of garnet are present. The earlier one exhibits garnet porphyroblasts which have abundant hornblende and plagioclase inclusions and are rimmed by recrystallized plagioclase and biotite, and the later one is characterized by euhedral garnets which are less abundant than the porphyroblasts. Euhedral garnet contains no inclusions and only occurs within plagioclase- and quartz-rich bands, suggesting that they are associated with plagioclase recrystallization. Microprobe analyses reveal no compositional differences either between garnet rims and cores or between different garnet generations (Table 2). Plagioclase is andesine ($An_{31-46}Ab_{52-67}Or_{1-2}$) (Table 2) and is recrystallized in all samples. From the least sheared sample (PS50, Fig. 3a) to the most sheared sample (PS60, Fig. 3c), both hornblende and plagioclase do not show systematic modal variations (Table 1). Pyroxene and garnet, however, are nearly completely consumed in the most sheared sample (PS60), by reaction to hornblende and plagioclase, respectively, indicating that deformation occurred under retrograde conditions. Biotite and muscovite are present as minor phases. Accessory minerals include allanite, monazite, apatite, zircon, and ilmenite.

In the mafic layers, no feldspar porphyroblasts are present, but the outlines of polycrystalline plagioclase aggregates indicate the shape of plagioclase porphyroblasts prior to complete recrystallization. Polycrystalline plagioclase aggregates commonly display ribbon shapes. The recrystallized plagioclase grains (100–300 μm) possess strain-free equant shapes with straight boundaries and triple junction contacts (Fig. 3c), indicating that they were deformed or experienced recovery and annealing at high temperature (White and Mawer, 1986; Ji and Mainprice, 1990). Quartz also experienced complete recrystallization. Individual quartz grains do not show undulatory extinction or subgrains. In thin section, the boundary between the mafic and felsic layers is sharp on a mm scale.

Felsic layer

The felsic layer (Fig. 3d–f) consists mainly of feldspar (51–56%), biotite (17–21%) and quartz (19–29%) (Table 1). Repetitious biotite-, quartz-, and plagioclase-rich bands define the foliation. Hornblende and garnet are only present in the highly sheared samples (PS10 and PS70), and occur close to the contacts with mafic layers in thin section. The weakly sheared samples (PS80 and PS40) contain abundant K-feldspar (14–20%), but in highly sheared samples (PS10 and PS70) in the same layer, plagioclase ($An_{22-29}Ab_{69-}$

Table 1. Modal mineralogy of analysed samples*

	PS50	PS30	PS20	PS60	PS10	PS70	PS40	PS80
	mafic layer				felsic layer			
quartz	2.8	1.6	7.8	4.0	24.4	18.8	25.4	29.3
plagioclase	27.0	38.0	14.2	37.0	52.0	50.2	33.0	39.6
K-feldspar	—	—	—	—	3.8	0.8	19.4	14.0
biotite	2.8	2.0	—	2.8	19.2	19.4	21.0	17.1
hornblende	51.2	52.0	60.0	57.0	tr	10.8	—	—
muscovite	—	2.2	—	—	—	—	—	—
garnet	10.6	1.2	12.4	—	0.6	—	—	—
ilmenite	2.0	1.6	3.8	1.6	—	—	0.8	—
epidote	—	0.8	—	—	—	—	—	—
pyroxene	3.6	0.6	tr†	tr	—	—	—	—
calcite	—	—	1.6	—	—	—	—	—
apatite	—	tr	tr	tr	tr	tr	tr	—
allanite	—	—	tr	tr	tr	tr	tr	tr
zircon	tr	tr	—	—	tr	—	tr	tr
monazite	—	tr	tr	—	tr	tr	tr	tr
specific gravity	3.11	3.01	3.05	2.90	2.68	2.73	2.71	2.65
D(cm)‡	140	110	50	0	0	15	60	130

*N = 500; †tr < 0.5%; ‡D is the distance to the shear zone.
PS60 and PS10 are mafic and felsic mylonites, respectively.

Table 2. Representative analyses of metamorphic minerals

	Garnet						Hornblende			Biotite			Plagioclase					K-spar	
layer	mafic				felsic		mafic			mafic		felsic	mafic			felsic		felsic	
samp.*	PS50		PS30		PS10		PS50		PS30	PS50	PS30	PS10	PS50	PS30	PS70	PS80	PS10	PS80	PS10
phase†	R		P		P		R	P	R	R			R			R		P	R
	core	rim			core	rim													
SiO_2	37.76	37.91	37.77	37.59	37.50	39.71	39.78	40.91	35.83	37.01	34.77	60.36	60.30	61.74	62.84	62.61	64.27	64.7	
Al_2O_3	20.69	21.04	20.65	21.06	20.98	20.88	15.67	15.76	16.35	14.98	16.44	16.27	25.51	24.51	23.20	23.63	23.83	18.99	18.66
TiO_2	0.01	0.00	0.49	0.06	0.01	0.01	1.88	1.54	1.22	4.57	1.02	1.90	ND	ND	ND	ND	ND	ND	ND
FeO	28.21	28.48	30.10	27.13	29.85	30.12	17.54	17.47	16.87	19.35	16.97	21.93	0.35	1.02	0.05	0.06	0.21	0.02	0.24
MnO	1.45	1.48	1.75	1.24	1.55	1.56	0.06	0.11	0.17	0.02	0.07	0.16	ND	ND	ND	ND	ND	ND	ND
MgO	4.62	4.63	3.26	4.74	4.20	4.20	9.30	9.20	9.61	12.71	13.74	10.10	ND	ND	ND	ND	ND	ND	ND
CaO	7.79	8.07	7.34	8.67	7.63	7.47	11.59	12.07	12.09	ND	ND	ND	7.41	6.35	4.31	4.41	4.56	0.02	0.11
Na_2O	ND	ND	ND	ND	ND	ND	1.54	1.72	1.62	0.09	0.01	0.08	6.76	7.41	8.80	8.52	8.25	0.61	0.03
K_2O	ND	ND	ND	ND	ND	ND	1.40	1.19	0.97	10.01	9.97	10.04	0.34	0.23	0.16	0.17	0.44	15.94	17.93
F	0.00	0.00	0.00	0.00	0.00	0.00	0.00	0.00	0.01	0.00	0.00	0.00	ND	ND	ND	ND	ND	ND	ND
Cl	0.00	0.00	0.00	0.00	0.00	0.00	0.07	0.02	0.00	0.03	0.02	0.54	ND	ND	ND	ND	ND	ND	ND
Total	100.5	101.6	100.9	100.7	101.8	101.7	98.7	98.9	99.9	97.6	95.3	95.8	100.7	99.8	98.3	99.6	99.9	99.9	101.7
Si	2.98	2.96	2.96	2.96	2.95	2.95	5.85	5.88	5.93	5.37	5.59	5.42	2.67	2.70	2.78	2.78	2.77	2.97	2.97
Al^{IV}	1.92	1.94	1.93	1.95	1.94	1.93	2.15	2.12	2.07	2.63	2.41	2.58	1.33	1.29	1.23	1.23	1.24	1.04	1.01
Al^{VI}	—	—	—	—	—	—	0.58	0.63	0.72	0.02	0.51	0.41	—	—	—	—	—	—	—
Ti	0.00	0.00	0.03	0.00	0.00	0.00	0.21	0.17	0.13	0.52	0.12	0.22	—	—	—	—	—	—	—
Fe	1.86	1.86	2.00	1.78	1.96	1.98	2.16	2.16	2.05	2.43	2.14	2.86	0.01	0.04	0.00	0.00	0.01	0.00	0.01
Mn	0.10	0.10	0.12	0.08	0.10	0.10	0.01	0.01	0.02	0.00	0.01	0.02	—	—	—	—	—	—	—
Mg	0.54	0.54	0.39	0.55	0.49	0.49	2.04	2.03	2.08	2.84	3.09	2.35	—	—	—	—	—	—	—
Ca	0.66	0.68	0.62	0.73	0.64	0.63	1.83	1.91	1.88	—	—	—	0.35	0.30	0.21	0.21	0.22	0.00	0.01
Na	—	—	—	—	—	—	0.44	0.49	0.46	0.03	0.00	0.02	0.58	0.64	0.77	0.73	0.71	0.06	0.00
K	—	—	—	—	—	—	0.26	0.22	0.18	1.92	1.92	2.00	0.02	0.01	0.01	0.01	0.02	0.94	1.05

*See sample localities in Fig. 2.
†R—recrystallized grain, P—porphyroclast or porphyroblast grain.

Table 3. Chemical compositions of whole rock samples

SAMPLE ID	PS50	PS30	PS20	PS60	error (1 s)	PS10	PS70	PS40	PS80	error (1 s)
		amphibolite layer					felsic layer			
SiO_2 (wt%)	50.1	48.8	47.2	49.2	0.06	65.9	71.6	72.0	73.5	0.07
TiO_2	1.57	1.62	2.19	1.25	0.005	0.79	0.5	0.42	0.36	0.00
Al_2O_3	13.4	13.6	12.8	14.5	0.01	12.6	12.0	12.0	11.8	0.03
Fe_2O_3*	15.0	15.7	17.2	12.7	0.015	7.00	5.28	4.43	4.46	0.005
Cr_2O_3	0.03	0.03	< 0.01	0.05	< 0.01	< 0.01	< 0.01	< 0.01	< 0.01	—
MnO	0.22	0.29	0.26	0.18	0.00	0.08	0.07	0.05	0.06	0.00
MgO	6.44	6.29	5.96	8.30	0.08	2.58	1.79	1.15	1.31	0.005
CaO	9.30	9.16	9.83	8.64	0.005	3.18	1.82	1.45	1.46	0.005
Na_2O	2.96	2.65	2.37	2.95	0.01	3.19	2.95	2.50	2.36	0.03
K_2O	0.70	0.77	1.26	1.31	0.005	2.62	3.78	4.43	4.87	0.02
P_2O_5	0.31	0.35	0.53	0.33	0.00	0.17	0.09	0.07	0.06	0.00
LOI	0.10	0.40	0.60	0.70	—	0.55	0.35	0.35	0.01	—
Total	100.1	99.75	100.3	100.2	—	98.84	100.40	99.03	100.40	—
Co (ppm)	39	36	42	43	0.2	13	7	3	4	0.2
Cr	180	170	130	280	0.05	100	98	100	86	0.05
Cs	< 1	< 1	< 1	7	0.1	3	4	1	< 1	0.1
Cu	53.8	55.1	100	52.4	—	64.3	48.9	22.3	22.3	—
Hf	5	5	4	4	0.05	10	14	14	15	0.05
Li	< 10	< 10	10	20	—	10	< 10	20	< 10	—
Nb	20	10	10	< 10	10	20	10	10	10	10
Ni	61	60	44	140	—	20	11	6	4	—
Pb	< 2	< 2	< 2	< 2	—	2	< 2	< 2	< 2	—
Rb	< 10	< 10	< 10	30	10	70	110	80	100	10
Ba	210	180	210	360		860	1000	830	850	
Sr	250	220	210	260	10	230	180	110	140	10
Sc	40.2	35.2	42.4	27.5	0.04	12.3	7.4	6.8	6.1	0.04
Th	< 1	< 1	< 1	< 1	0.05	6	9	10	10	0.05
U	< 0.5	< 0.5	< 0.5	< 0.5	—	0.9	0.9	0.9	1	—
V	330	280	390	180	—	70	50	30	20	—
Zn	160	140	190	120	2	76	63	54	50	2
Zr	160	190	190	160	10	390	470	420	560	10
Y	50	50	60	30	10	60	40	50	50	10
La (ppm)	15.0	20.7	17.5	13.2	0.04	47.2	64.2	60.4	64.5	0.04
Ce	39	50	41	29	0.07	98	120	118	119	0.07
Nd	24	29	23	20	0.8	44	46	55	52	0.8
Sm	6.1	7.7	7.8	4.8	0.03	9.2	8.7	10.5	9.3	0.03
Eu	2.3	2.5	2.2	1.3	0.04	1.7	1.5	1.4	1.4	0.04
Tb	1.3	1.4	1.2	0.9	0.03	1.3	1.1	1.2	1.0	0.03
Yb	5	5.5	5.7	3	0.08	4.9	3.3	4.6	3.7	0.08
Lu	0.74	0.82	0.88	0.44	0.007	0.8	0.54	0.74	0.57	0.007
$\delta^{18}O$ (‰)	7.5	7.8	7.0	8.3		9.2	9.3	9.9	9.7	

*All iron is reported as Fe_2O_3.

$_{75}Or_{1-5}$; Table 2) becomes dominant (Fig. 3f), with only rare alkali feldspar porphyroblasts. The K-feldspar is more K-rich in the highly sheared samples ($Or \geq 99$) compared to the less sheared samples ($Or \approx 94$; Table 2).

In less sheared samples (PS80 and PS40), K-feldspar porphyroclasts (Fig. 3e) commonly show sweeping undulatory extinction and optically visible subgrains with saw-tooth boundaries, and are rimmed by fine-grained (80–100 μm) recrystallized plagioclase and K-feldspar grains. The recrystallized plagioclase and K-feldspar display strain-free equant grains with straight boundaries and triple junction contacts (Fig. 3f). Mono- and polycrystalline quartz ribbons define the *S*-surface. A *C*-surface is defined by strongly oriented fine-grained biotite (54 ± 15 μm). The *S–C* fabrics indicate a normal sense of shear, consistent with the outcrop scale offset (Fig. 2).

In the most sheared felsic sample (PS10), the sides of relict K-feldspar porphyroclasts are rimmed by myrmekitic intergrowths of oligoclase (An_{22-28}) and quartz, suggesting that they are the results of syn-deformation reactions at high temperature (Simpson and Wintsch, 1989). The dominant feldspar is recrystallized equant plagioclase grains that also show equant grain shapes and triple junction contacts (Fig. 3f). The abundance of recrystallized feldspar increases progressively with decreasing distance to the shear zone (Fig. 4). Because the felsic layer is dominated by relatively weak minerals (quartz and biotite), whereas the mafic layer is dominated by stronger minerals (feldspar and hornblende) the felsic layer was probably weaker than the mafic layer (Brodie and Rutter, 1985).

DEFORMATION AND METAMORPHIC CONDITIONS

In order to estimate the final equilibration pressures and temperatures of the assemblages in both the mafic

and felsic layers, hornblende, garnet, and biotite were analyzed by electron microprobe (Table 2). Fine-grained hornblende grains with triple junction grain boundaries and both retrograde porphyroblasts and euhedral neoblasts of garnet were analyzed. These minerals do not display zoning from rim to core (Table 2). The hornblende–garnet geothermometer of Graham and Powell (1984) yields a temperature of 647 ± 54°C ($n = 10$), and the garnet–biotite geothermometer of Ferry and Spear (1978) yields a temperature of 705 ± 72°C ($n = 9$). The garnet–rutile–ilmenite–plagioclase–quartz (GRIPS) geobarometer of Bohlen and Liotta (1986) yields a pressure of 9 kb at 700°C and 8 kb at 650°C. The geobarometer based on the total aluminum content of hornblende (Hammarstrom and Zen, 1986) yields a pressure of 10 ± 0.3 kb ($n = 6$). The temperature range (600°C–710°C) indicated by garnet–biotite and hornblende–garnet geothermometers is consistent with the mineral assemblages and fabric features, such as recrystallization and annealing of plagioclase. It is also consistent with the *P–T* conditions of the post-thrusting extension in the Grenville Province suggested by extensive thermobarometric studies in Parry Sound area and vicinity (Anovitz and Chase, 1990; Busch *et al.*, 1996). Thus, the normal shear zone was likely formed between 600–710°C and 8–10 kb during the post-thrusting extension. The high pressure indicated suggests a setting in the lower continental crust.

WHOLE ROCK GEOCHEMISTRY

Results

Whole rock chemical analyses were undertaken in order to evaluate the role of mass transfer processes during deformation. The data are presented in Table 3. As expected, the mafic and felsic layers have distinct compositions. The compositions of the mylonites, however, are different from either the mafic or the felsic protoliths. For example, felsic components (such as SiO_2, and K_2O) are lower and mafic components (such as CaO, Fe_2O_3, MgO and TiO_2) are higher in the felsic mylonite compared to the felsic protolith. Conversely, mafic components (CaO, Fe_2O_3, TiO_2) are lower and K_2O and MgO are higher in the mafic mylonite compared to the mafic protolith. The significance of these chemical changes is examined below.

Previous studies have interpreted compositional changes in mylonites with respect to protolith as the result of several distinct processes including mass transfer of mobile elements (Sinha *et al.*, 1986, 1988; O'Hara and Blackburn, 1989; Yang *et al.*, 1995), relative changes of immobile elements as a result of volume change (O'Hara, 1988; Newman and Mitra, 1993), and mechanical mixing between two or more lithologies (Evans and Chester, 1995). In order to evaluate the significance of the concentration changes in the mylonites, it is useful to examine the changes relative to an immobile frame of reference. The elements used as reference should be geochemically coherent (i.e. have similar crystal–chemical behavior), and have a low analytical error relative to their concentration. Vanadium, Sc and Ti and the REE are commonly believed to be immobile during metamorphism at relatively high temperature (Evans and Landergren, 1970; Frondal, 1970; O'Hara and Blackburn, 1989; Rollinson, 1989). The LREE display a gradual change in radius and behave coherently as a group and the transition elements (V, Sc and Ti) also have similarities in their crystal–chemical behavior. These elements have low analytical error (Table 3). Scandium, V and Ti tend to be enriched in mafic minerals, such as garnet, ilmenite, hornblende and biotite (Table 2; Evans and Landergren, 1970; Frondal, 1970) and the LREE tend to be enriched in accessory minerals associated with felsic components.

Rare earth elements (REE)

The REE data for the mafic and felsic layers (normalized to chondritic values) show two contrasting patterns (Fig. 5), in which the felsic layer is LREE-enriched relative to the mafic layer. When the mylonites are normalized to their respective protoliths, the REE show more complex patterns (Fig. 6a & b). In the felsic layer, the mylonite (PS10) shows depletion in LREE (La, Ce, Nd, Sm) and enrichment in HREE (Eu, Tb, Yb, Lu) and Y relative to the protolith, and the less sheared sample (PS40) shows minor changes in LREE and enrichments in Tb, Yb, and Lu (Fig. 6a). In the mafic layer, with the exception of PS20, the samples show roughly parallel patterns with different concentrations. The most sheared sample (PS60) shows depletion in all REE and Y relative to the protolith (PS50) (Fig. 6b). Sample PS30 displays a slight enrichment in all of REE, but no change in Y relative to the protolith. Sample PS20 is enriched in La, Ce, Sm, Yb, Lu, and Y, with minor change in Nd, Eu, Tb (Fig. 6b).

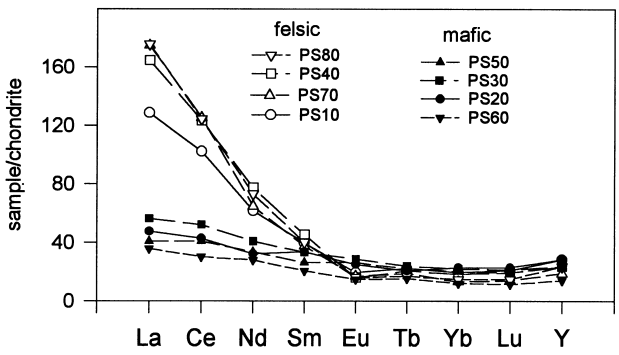

Fig. 5. Chondrite-normalized REE patterns of felsic samples (open symbols) and mafic samples (solid symbols). Chondritic REE values from Taylor and McLennan (1985). The felsic layer is LREE-enriched relative to the mafic layer.

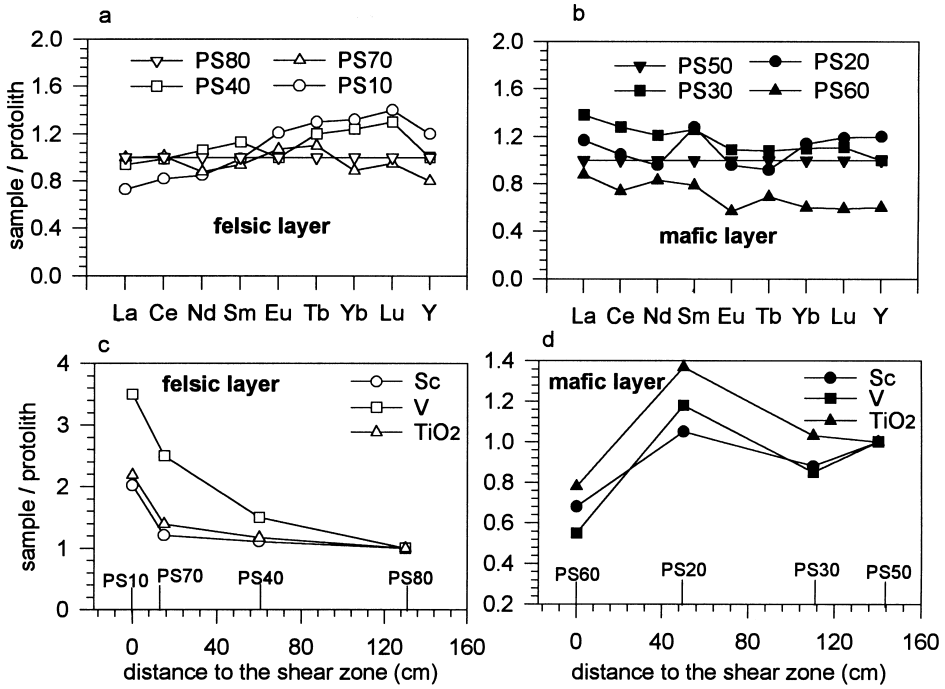

Fig. 6. Variation in REE and selected elements normalized to the least sheared samples. (a) REE pattern of felsic mylonites normalized to the felsic protolith (PS80). (b) REE pattern of mafic mylonites normalized to the mafic protolith (PS50). (c) Variation of Ti, V and Sc in the felsic samples normalized to PS80, as a function of distance to the shear zone. (d) Same as (c) for the mafic samples normalized to PS50.

The magnitude of these variations is about $\pm 30\%$ (Fig. 6a & b) and in the case of the HREE, which have low concentrations in both layers (Fig. 5), small modal changes in accessory minerals such as ilmenite, apatite, and zircon (Table 1) may explain much of this variation.

Titanium, vanadium, scandium

The felsic mylonites show progressive enrichment in TiO_2, Sc, and V with progressive deformation (Fig. 6c). On the other hand, the mafic mylonites show depletion in TiO_2, Sc, and V with progressive deformation (with the exception again of PS20, Fig. 6d). Sample PS20 contains more hornblende, garnet and ilmenite compared to the other samples (Table 1), minerals which accommodate Ti, Sc and V, and this may explain the anomalous position of PS20 on Fig. 6(d). Overall, TiO_2, Sc, and V display contrasting behavior in the mafic and felsic layers with distance to the shear zone (Fig. 6c & d). Because the concentrations of TiO_2, Sc and V are substantially higher in the mafic layer compared to the felsic layer, contamination of the felsic layer by the mafic layer would result in an increase in abundance of these elements in the felsic layer, and conversely, contamination of the mafic layer with the felsic layer would result in a decrease in the abundance of these elements in the mafic layer, as observed. This suggestion is supported by the presence of rare garnet and hornblende only in the most sheared felsic samples, noted above. The garnets in the mafic and felsic layers are compositionally similar (Table 2).

The above variations are also displayed by $\delta^{18}O$ values. The protoliths of the felsic and mafic layers have $\delta^{18}O$ values of 9.2% and 7.5%, respectively. $\delta^{18}O$ values show an overall increase in the mafic mylonites and an overall decrease in the felsic mylonites compared to their respective protoliths (Table 3), again supporting mixing between a low $\delta^{18}O$ end-member (mafic layer) and a high $\delta^{18}O$ end-member (felsic layer).

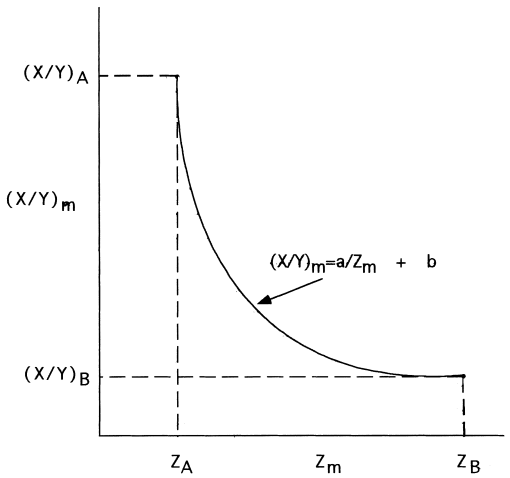

Fig. 7. Plot of ratios of elements or isotopes (X/Y) vs element concentration (Z) for two component mixing of end members A and B.

TWO-COMPONENT MIXING

Under closed system conditions, element concentrations and element ratios of a mixture of two com-

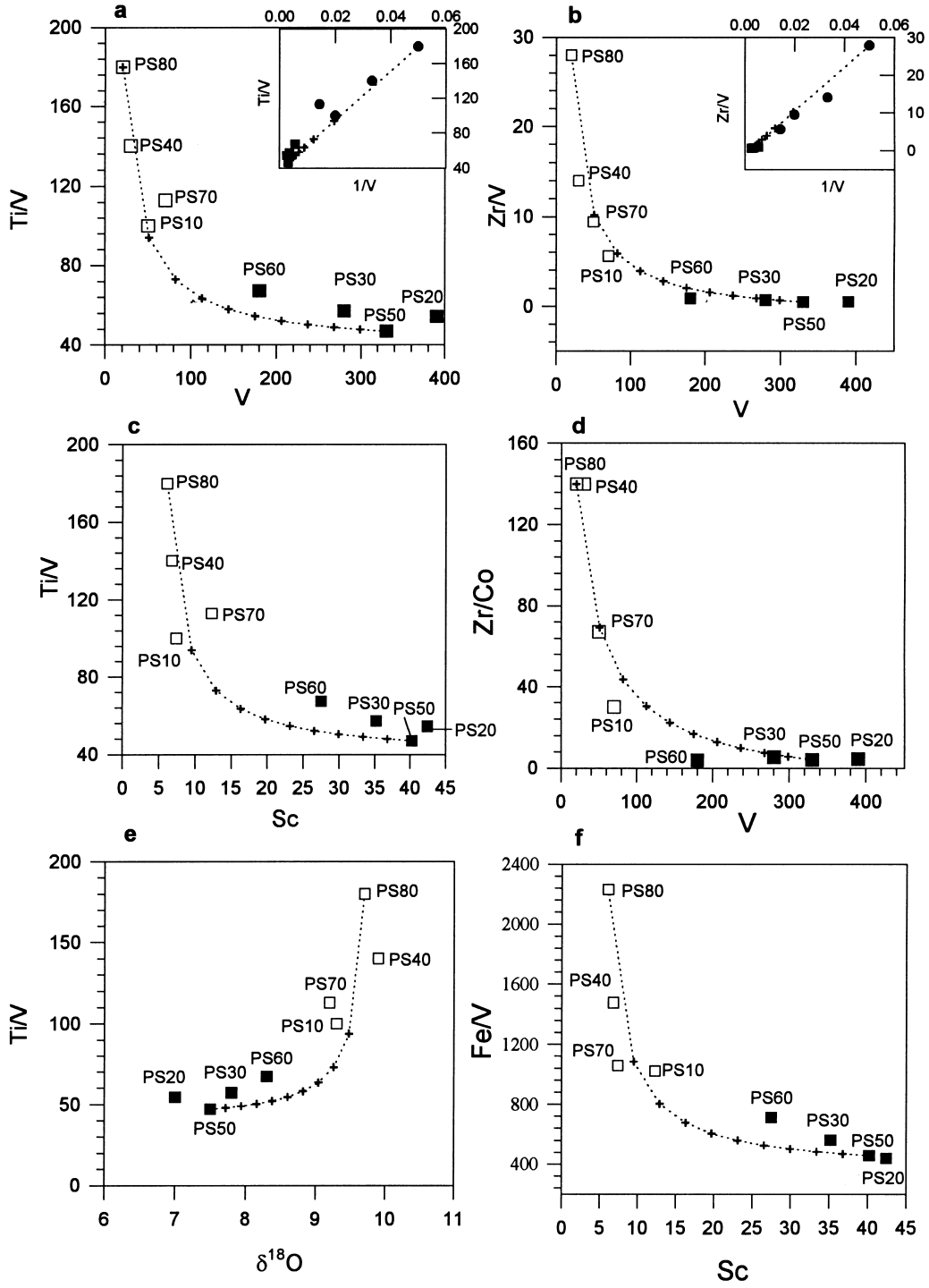

Fig. 8. Plots of selected observed element ratios vs element concentrations. Filled symbols are mafic sample; open symbols are felsic sample. (a) TiO_2/V vs V, the curve is defined by $(TiO_2/V)_m = 2832.3/V_m + 38.4$ (inset shows the plot of Ti_m vs 1/V). (b) Zr/V vs V, the curve is defined by $(Zr/V)_m = 585.9/V_m - 1.3$ (inset shows the plot of Zr/V vs V). (c) TiO_2/V vs Sc, the curve is defined by $(TiO_2/V)_m = 956.6/Sc_m + 23.2$. (d) Zr/Co vs V, the curve is defined by $(Zr/Co)_m = 2893.4/V_m - 4.7$. (e) TiO_2/V vs $\delta^{18}O$, the curve is defined by $(TiO_2/V)_m = -4399.1/(\delta^{18}O)_m + 633.5$. (f) Fe_2O_3/V vs Sc, the curve was defined by $(Fe_2O_3/V)_m = 12745.7/Sc_m + 38.4$. The least sheared felsic (PS80) and mafic (PS50) samples are treated as end-members. Sample PS20 is anomalous and plots beyond the mafic end-member in all the plots.

ponents depend only on the mass fraction of the end-members.

Plots of isotopic ratios or element ratios vs concentration have been successfully used in studying the petrogenesis of igneous rocks involving mixing of source rocks (Langmuir *et al.*, 1978; Faure, 1986). Considering two end-members *A* and *B* and three elements, *X*, *Y* and *Z*, on a plot of *X*/*Y* vs *Z* (Fig. 7), the mixing curve will be a hyperbola with the general form (Langmuir *et al.*, 1978; Faure, 1986):

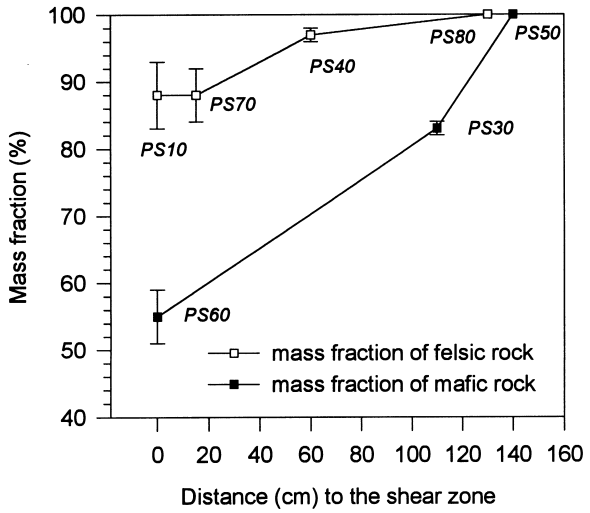

Fig. 9. The plot of mixing fraction as a function of the distance to the shear zone. X_m represents the mass fraction of mafic rock in the mafic layer, and X_f represents the mass fraction of felsic rock in the felsic layer. The mass fraction was derived from the plots of element ratio vs concentration and the mixing curves (Fig. 8). The error bars represent the uncertainty of the calculated mass fraction from different plots in Fig. 8.

$$(X/Y)_m = a/Z_m + b \quad (1)$$

where coefficients a and b can be obtained from the end-members (Fig. 8):

$$a = Z_A Z_B[(X/Y)_B - (X/Y)_A]/(Z_A - Z_B) \quad (2)$$

$$b = [Z_A(X/Y)_A - Z_B(X/Y)_B]/(Z_A - Z_B) \quad (3)$$

On plots of element ratios vs element concentration (e.g. Ti/V vs V; Ti/V vs Sc; Zr/V vs V; Zr/Co vs V; and Fe/V vs Sc) the deformed samples show hyperbolic trends (Fig. 8). They plot near the theoretical mixing curve derived from equations (1)–(3) using samples PS50 for the protolith mafic layer and PS80 for the protolith felsic layer as end-members. On a plot of TiO_2/V vs $\delta^{18}O$, the deformed samples also plot near the mixing curve (Fig. 8e). The end-members used are farthest from the shear zone (Fig. 2b) and show the least amount of recrystallization (Fig. 4). Sample PS20 lies beyond one of these end members, and in this regard is anomalous.

If Ti, V, Zr and Co were mobile, it is unrealistic to expect the Ti/V, Fe/V, Zr/V and Zr/Co ratios to lie on a mixing curve. If, on the other hand, they were immobile, the changes in their ratios cannot be due to either volume change or other fluid-related processes. We therefore interpret the trends in Fig. 8 as evidence that mixing took place between the two lithologies in the shear zone. This interpretation is supported by the increase in mafic components observed in the felsic mylonites and of felsic components in the mafic mylonites described above. The mixing fractions of the variously sheared samples, with the exception of PS20, can be obtained from the location of the samples on the mixing line (Fig. 8). These fractions are shown as a function of distance to the shear zone in Fig. 9 which illustrates an increase in mixing with progressive deformation. This suggests that mixing and shearing are related (see Discussion). It can be seen that the felsic mylonite can be derived from $88 \pm 5\%$ felsic and $12 \pm 5\%$ mafic components, and the mafic mylonite can be derived from $55 \pm 4\%$ mafic and $45 \pm 4\%$ felsic components.

FLUID-ASSISTED MASS TRANSFER

Based on the mixing fractions and the compositions of the end-members, equation (A7) can be used to calculate the major and trace element compositions of deformed samples, assuming closed system conditions. If the calculated and observed compositions agree, then closed system mixing is supported. If on the other hand, substantial disagreement exists, then open system behavior is implied. Figure 10 compares the observed data and calculated compositions (based on mixing fractions derived above) of major and trace elements for the felsic and mafic samples. Using PS 50 and PS 80 as end-members, two samples collected outside the shear zone (PS70 and PS30) have mixing fractions of $88 \pm 4\%$ felsic + $12 \pm 4\%$ mafic rocks and $17 \pm 1\%$ felsic + $83 \pm 1\%$ mafic rocks, respectively. Most elements (major, REE, and trace) plot along the constant mass diagonal (Fig. 10a & c). The relatively good fits between calculated and observed data for these samples indicates that these samples experienced little or no fluid-assisted mass transfer. In contrast, in the most sheared mafic and felsic samples (PS 10 and PS 60), few elements plot along the constant mass line (Fig. 10b & d) indicating that the shear zone was an open system and involved *both* mixing and fluid-assisted mass transfer of mobile elements.

On the plot of felsic mylonite (PS 10) vs its calculated mixed protolith, TiO_2, Fe_2O_3 V, Sc, and HREE (Eu, Tb, Yb, Lu) define an isocon whose slope is somewhat steeper than the constant mass isocon (Fig. 10b). Other elements, CaO, MgO, Na_2O, Co, Y, Zn and Sr, also plot near this isocon. However, K_2O, SiO_2, Al_2O_3, LREE, Zr, Hf, Rb, and Ba fall below the isocon to varying degrees. In the case of mafic mylonite (PS 60) vs its calculated protolith, TiO_2, Fe_2O_3, Al, Sc, Yb and Lu also define an isocon with Na_2O, V, Tb, Cu and Zn plotted near this line (Fig. 10d). CaO, MgO, and P_2O_5 plot above this isocon, and other elements scatter conspicuously below this isocon and the constant mass line. The isocons defined by Fe, Ti, V, Sc, and HREE in Fig. 10(b & d) are interpreted to represent an immobile isocon.

Based on mass balance of these immobile elements, the volume factor duing mylonitization can be obtained from (Gresens, 1967; Grant, 1986)

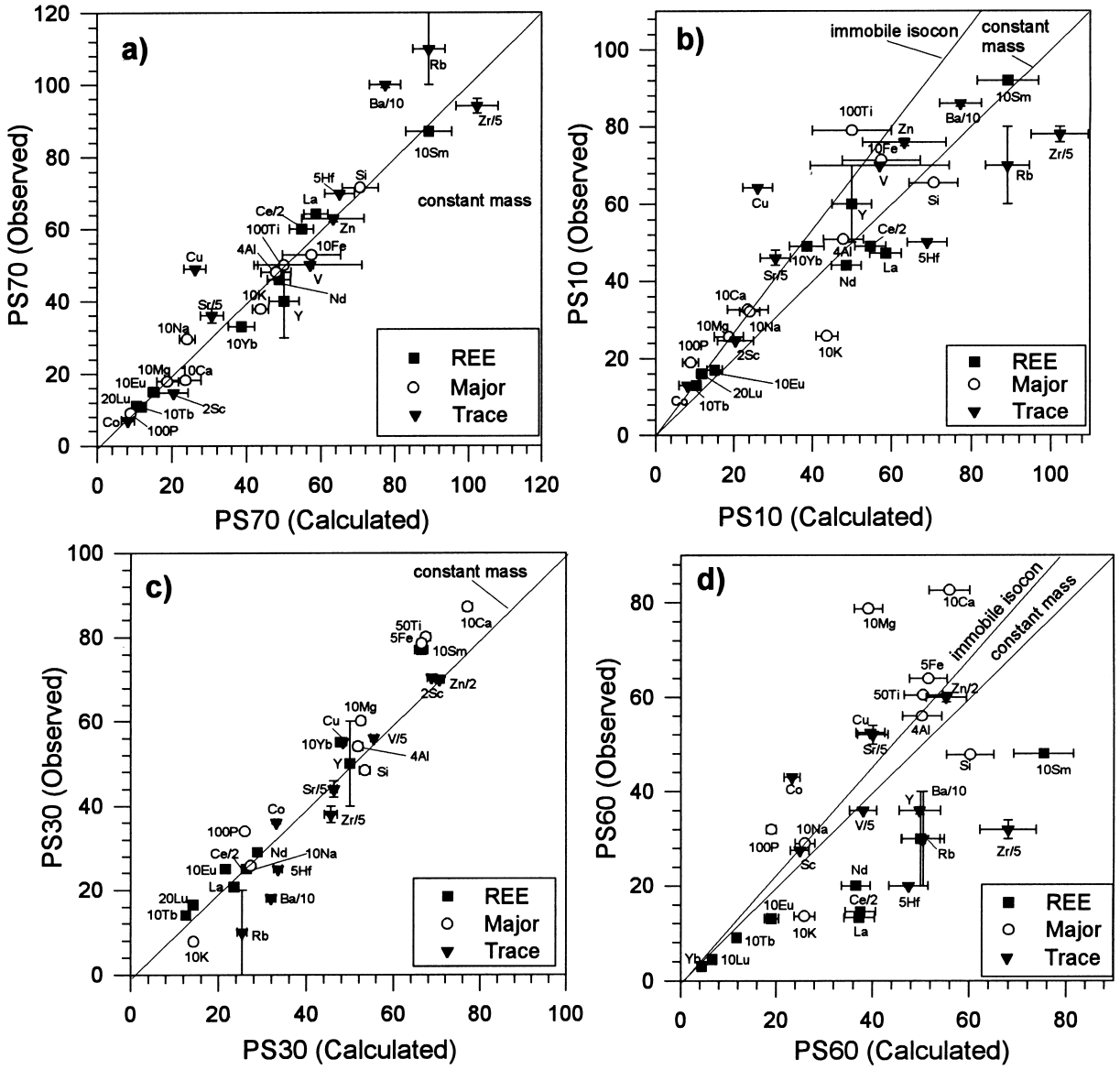

Fig. 10. Isocon diagram of the observed concentrations vs the calculated concentrations for proto-mylonites (a & c) and mylonites (b & d). The calculated compositions are derived from two-component mixing under closed system conditions. Vertical error bars represent analytical error (1σ) and horizontal error bars represent calculation uncertainty resulted from the mass fraction uncertainty.

$$f_v = V^F/V^I = C_i^P/C_i^M * \rho^P/\rho^M \quad (4)$$

where V^I and V^F are initial and final volumes of altered rocks, respectively; $C^P{}_i$ and $C^M{}_i$ are concentrations of element i in protolith and mylonite, respectively; ρ^P and ρ^M are densities of protolith and mylonite. The term $C^P{}_i/C^M{}_i$ can be determined from the slope of immobile element isocon in Fig. 10. The initial state (protolith) is assumed to be the rock resulting from mixing without fluid-assisted mass transfer. The density of the protolith can be obtained from the densities of the end-members through equation (A2) by assuming that there was no volume change during mixing in a closed system; this equation yields densities for felsic and mafic protoliths of 2.70 ± 0.3 and 2.90 ± 0.2 g/cm^3, respectively. Consequently, a volume loss of 24% for the felsic mylonite and 13% for the mafic mylonite is derived from the immobile element isocon (Fig. 10b & d). The net chemical changes due to mass transfer can be determined from Gresens' (1967) equation. The calculations yield the following two mass balance equations:

$$\begin{aligned} 100\,\text{g } \textit{felsic mixture} + 0.3\,\text{g LOI} &= 73.9\,\text{g} \\ \textit{felsic mylonite} + 2.2\,\text{g } Al_2O_3 &\\ + 21.7\,\text{g } SiO_2 + 2.5\,\text{g } K_2O & \end{aligned} \quad (5)$$

$$\begin{aligned} 100\,\text{g } \textit{mafic mixture} + 1.6\,\text{g CaO} + 2.9\,\text{g MgO} &\\ + 0.5\,\text{g LOI} = 85.5\,\text{g } \textit{mafic mylonite} &\\ + 18.6\,\text{g } SiO_2 + 1.42\,\text{g } K_2O + 0.4\,\text{g } Al_2O_3. & \end{aligned} \quad (6)$$

Equations (5) and (6) indicate losses of SiO_2, Al_2O_3,

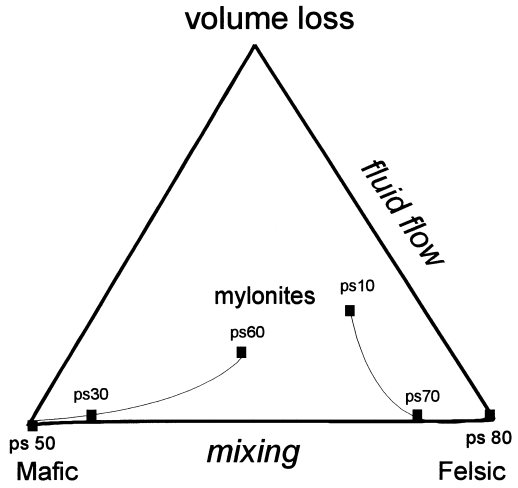

Fig. 11. Mixing-volume loss plot. Closed system mixing moves the protolith compositions horizontally along the base of the triangle and open system behavior will move the rocks vertically. The data are consistent with a process in which mixing and fluid influx are related.

and K_2O from the felsic layer and SiO_2 from the mafic layer. On the other hand, the mafic layer gained a significant amount of CaO and MgO during mylonitization. The loss of K_2O from the felsic mylonite is consistent with the observed change from microcline to plagioclase in the felsic layer with increasing deformation. In summary, the chemical composition of the mylonites may be explained by processes including both mixing of end-member lithologies and fluid-assisted mass transfer.

DISCUSSION

Fluid-to-rock ratios

The mass transfer of mobile elements implied by equations (5) and (6) requires a fluid influx to remove and/or add elements to mylonites and the retrograde reactions described above are consistent with the presence of a fluid phase. Based on the net changes of SiO_2 and the solubility of SiO_2, a minimum fluid-to-rock mass ratio may be calculated if the P/T conditions and saturation of the fluid with respect to SiO_2 are known. The equation of O'Hara and Blackburn (1989) is used to determine fluid-to-rock volume ratio:

$$(\text{Fluid/Rock}) = L_{si}/C_{si}(1 - S) \qquad (7)$$

Where L_{si} is the net change of SiO_2; C_{si} is the solubility of SiO_2 at the P/T condition of deformation; S is the fractional saturation of fluid with respect to SiO_2. It is clear from equation (7) that a minimum fluid-to-rock ratio is obtained assuming a totally unsaturated fluid ($S = 0$), and an infinitely large ratio is obtained for a fully saturated fluid ($S = 1$). Using the experimental data of Manning (1994), the solubility of SiO_2 at 700°C and 10 kbar is approximately 3.6 wt%. Based on the net SiO_2 loss, 21.7 g/100 g rock, indicated by equation (5), fluid-to-rock ratios of 6:1, 12:1 and 60:1 are obtained, assuming 0%, 50%, and 90% saturation of the fluid. Because oxygen is expected to be mobile under these conditions, but $\delta^{18}O$ values of the samples plot near a closed system mixing curve (Fig. 8e), the implication is that the fluid influx occurred prior to mixing or that the fluid was in O isotope equilibrium with the host-rocks during mixing. This raises the possibility, discussed below, that the fluid played a role in the mixing process.

Although the intermediate deformed felsic and mafic samples, PS70 and PS30, were collected only 15 cm and 110 cm away from the shear zone, respectively, and display deformation fabric and grain-size reduction relative to their protoliths (Fig. 4), they show only minor fluid-associated chemical changes compared to the felsic and mafic mylonites collected within the shear zone (Fig. 10a & c). This implies that fluid-rock interaction was largely confined to the shear zone, and represents channelized fluid flow.

Mixing and strain weakening

Mixing between rocks of contrasting composition apparently had the ability to significantly change the chemical and mineralogical composition of the mylonites. The process may also have affected the strength of the mylonites. The bulk strength of a rock depends on the strength of constituent minerals and their mass fraction in a non-linear fashion (Handy, 1990). Phases which are sufficiently abundant to form an interconnected network have an important influence on the bulk strength (Handy, 1990). The felsic layer in this study contains minerals such as biotite and quartz which make up between 37% and 43% of the felsic mylonites, and under upper amphibolite conditions, these minerals are likely to be fully plastic. The mafic layer on the other hand is dominated by hornblende and feldspar with $<5\%$ quartz or biotite (Table 1) and was probably stronger at the P–T conditions of mylonitization. This is consistent with experimental and natural deformation studies which indicate that feldspar is generally weaker than hornblende at amphibolite facies conditions (>550°C, e.g. Brodie and Rutter, 1985; Hacker and Christie, 1990), but both minerals are stronger than either quartz or mica. In the shear zone, the felsic mylonite consists of $12 \pm 5\%$ mafic protolith and $88 \pm 5\%$ felsic protolith, whereas the mafic mylonite consists of $55 \pm 4\%$ felsic protolith and $45 \pm 4\%$ mafic protolith (Fig. 9). The mixing process, therefore, resulted in addition of a greater proportion of felsic components (55 wt%) to the mafic layer compared to the addition of only 12 wt% mafic components to the felsic layer. Insofar as the felsic components form an interconnected network and were likely weaker than the mafic components, an overall weakening of the mixed rock would have occurred. This process of shearing–mixing–weakening causing

further shearing and weakening may be one of the strain weakening mechanisms which operated at the outcrop scale in this study.

Mechanical vs chemical mixing

The observed chemical changes are interpreted as due to mixing between the felsic and mafic layers and also to mass transfer involving a fluid phase. During mylonitization, two types of mixing are possible; namely, mechanical mixing due to shearing between the two contrasting lithologies and chemical mixing due to mass transfer of components. In this study, the proportions of mixing were identified on the assumption of immobility of certain elements, regardless of the amount of fluid infiltration. Based on this assumption, the mixing must reflect physical mixing of these immobile elements, rather than their chemical transport. The presence of minor amounts of relict hornblende and garnet in the more deformed felsic samples is physical evidence that the mafic layer contributed minerals to the felsic layer. That the rare garnet in the felsic layer is similar in composition to the garnet in the mafic layer (Table 2) is consistent with mechanical mixing of garnet due to shearing, rather than chemical transport of garnet components from mafic to felsic layers. In the latter case, it is likely that a garnet growing in a felsic host would be chemically distinct from garnet growing in a mafic host.

The change from dominantly K-feldspar to dominantly plagioclase with progressive deformation of the felsic layer is consistent with either mixing of plagioclase from the mafic layer with the felsic layer, or alternatively, loss of K and gain of Na and Ca in the felsic layer. Because open system fluid-assisted mass transfer was also involved during mylonitization, differentiating between mechanical and chemical mixing in this case is difficult. In the case of less deformed samples, however, simple mixing under closed system conditions satisfactorily explains the major, minor and trace element concentrations (Fig. 10a & d). Given the likely different mobilities of these elements it is unrealistic to expect that chemical transport would result in a pattern similar to that predicted by two component mixing. A process is envisioned, therefore, in which shearing juxtaposed the two contrasting lithologies resulting in mechanical mixing of mafic and felsic protolith samples.

The absence of zoning in either garnet or hornblende suggests that intercrystalline diffusion was sufficient to homogenize these phases. In addition, grain-size reduction of hornblende and feldspar during recrystallization in both layers would increase the grain boundary cross-sectional area, thereby enhancing grain boundary diffusion (Farver and Yund, 1995). These diffusive processes would tend to homogenize the rocks, possibly erasing evidence for the nature of the mixing process. The presence of a separate fluid phase would clearly enhance transport processes during mixing.

The relative roles of mixing and mass transfer processes can be represented on a mixing-volume loss diagram (Fig. 11). The end member protolith compositions plot at the apices at the base of the triangle. Samples outside the shear zone (PS30 and PS70) plot along the base line, indicating closed system mixing. Mylonite samples plot off the base line indicating open system behavior. Mafic mylonite sample PS60 shows higher proportions of mixing in addition to 13% volume loss, whereas the felsic mylonite (PS10) shows similar mixing proportions as PS70 and a volume loss of 24%. The data are consistent with the interpretation that fluid influx and mixing are related processes, but further studies are required to identify the nature and mechanisms of these interactions.

In conclusion, the available evidence suggests that, in the case of the less deformed samples outside the mylonite zone, the mixing process was limited, and was largely mechanical, rather than chemical, in nature. In the case of the mylonites, deformation involved mass transfer and mixing processes, and the mixing may have been enhanced by the presence of the fluid phase. Regardless of the exact mechanisms by which these processes interacted, a positive result of this study is that mixing can be distinguished from mass transfer processes, provided an immobile frame of reference can be identified. Because of the small scale and limited sample base of this study it is unclear how important these processes are in other tectonic settings, and on what scale they operate, and whether fluid infiltration, in general, promotes mixing.

Acknowledgements—This study was supported by NSF grant EAR-9316954 to KOH and DPM. The assistance of Henry Francis and Mark Thompson in XRF analysis at the Kentucky Geological Survey is gratefully acknowledged. Journal reviews by Simon Cox, Michael Williams and an anonymous reviewer were appreciated.

REFERENCES

Anovitz, L. M. and Chase, C. G. (1990) Implications of post-thrusting extension and underplating for *P–T–t* paths in granulite terranes: A Grenville example. *Geology* **18,** 466–469.

Anovitz, L. M. and Essene, E. J. (1990) Thermobarometry and pressure–temperature paths in the Grenville Province of Ontario. *Journal of Petrology* **31,** 197–241.

Beach, A. (1980) Retrogressive metamorphic processes in shear zone with special reference to the Lewisian Complex. *Journal of Structural Geology* **2,** 257–263.

Bohlen, S. R. and Liotta, J. J. (1986) A barometer for garnet amphibolites and garnet granulites. *Journal of Petrology* **27,** 1025–1034.

Brodie, K. H. and Rutter, E. H. (1985) On the relationships between deformation and metamorphism, with special reference to the behavior of basic rocks. In *Metamorphic Reactions Kinetic, Textures and Deformation*, eds A. B. Thompson and D. C. Rubie, pp. 138–179. Springer-Verlag, New York.

Busch, J. P., Essene, E. J. and van der Pluijm, B. A. (1996) Evolution of deep-crustal normal faults: constraints from thermobarometry in the Grenville orogen, Ontario, Canada. *Tectonophysics* **265,** 83–100.

Davidson, A. (1984) Identification of ductile shear zones in the southwestern Grenville Province of the Canadian Shield. In

Precambrian Tectonics Illustrated, eds A. Kroner and R. E. Greiling, pp. 263–279. Schweizerbart'sche Verlagsbuchhandlung.

Davidson, A., Culshaw, N. G. and Nadeau, L. (1982) A tectonometamorphic framework for part of the Grenville Province, Ontario. In *Current Research, Part A, Geological Survey of Canada paper 82-1A*, pp. 175–190.

Evans, H. T. Jr and Landergren, S. (1970) Vanadium. In *Handbook of Geochemistry*, eds K. H. Wedepohl, C. W. Correns, D. M. Shaw, K. K. Turekian and J. Zemann, pp. 23-A-1–23-O-1. Springer-Verlag, New York, **II/2**.

Evans, J. P. and Chester, F. M. (1995) Fluid-rock interaction in faults of the San Andreas system: inferences from San Gabriel fault rock geochemistry and microstructures. *Journal of Geophysics Research* **100,** 13,007–13,020.

Faure, G. (1986) *Principles of Isotope Geology*. John Wiley & Son, New York.

Farver, J. R. and Yund, R. A. (1995) Grain boundary diffusion of oxygen, potassium and calcium in natural and hot-pressed feldspar aggregates. *Contributions to Mineralogy and Petrology* **118,** 340–355.

Ferry, J. M. and Spear, F. S. (1978) Experimental calibration of the partitioning of Fe and Mg between biotite and garnet. *Contributions to Mineralogy and Petrology* **66,** 113–117.

Frondal, C. (1970) Scandium. In *Handbook of Geochemistry*, eds K. H. Wedepohl, C. W. Correns, D. M. Shaw, K. K. Turekian and J. Zemann, pp. 21-A-1–21-O-1. Springer-Verlag, New York, **II/2**.

Glazner, A. F. and Bartley, J. M. (1991) Volume loss, fluid flow and state of strain in extensional mylonites from the central Mojave Desert California. *Journal of Structural Geology* **13,** 587–594.

Goddard, J. V. and Evans, J. P. (1995) Chemical changes and fluid-rock interaction in faults of crystalline thrust sheets, Northwestern Wyoming, U.S.A. *Journal of Structural Geology* **17,** 533–547.

Graham, C. M. and Powell, R. (1984) A garnet–hornblende geothermometer: calibration, testing, and application to the Pelona Schist, Southern California. *Journal of Metamorphic Geology* **2,** 13–31.

Grant, J. A. (1986) The isocon diagram—A simple solution to Gresens' equation for metasomatic alteration. *Economic Geology* **81,** 1976–1982.

Gresens, R. L. (1967) Composition–volume relationships of metasomatism. *Chemical Geology* **2,** 47–65.

Hacker, B. R. and Christie, J. M. (1990). Brittle/ductile and plastic/cataclastic transitions in experimentally deformation and metamorphosed amphibolite. *Geophysical Monograph of the American Geophysical Union*. **56,** 127–147.

Hammarstrom, J. M. and Zen, E. (1986) Aluminum in hornblende: An empirical igneous geobarometer. *American Mineralogist* **71,** 1297–1313.

Handy, M. R. (1990) The solid-state flow of polymineralic rocks. *Journal of Geophysical Research* **95,** 8647–8661.

Hickman, S., Sibson, R. H. and Bruhn, R. (1995) Introduction to special section: Mechanical involvement of fluids in faulting. *Journal of Geophysical Research* **100**(B7), 12,831–12,840.

Janecke, S. U. and Evans, J. P. (1988) Feldspar-influenced rock rheologies. *Geology* **16,** 1064–1067.

Ji, S. and Mainprice, D. (1990) Recrystallization and fabric development in plagioclase. *Journal of Geology* **98,** 65–79.

Langmuir, C. H., Vocke, R. D., Jr., Hanson, G. N. and Hart, S. R. (1978) A general mixing equation with applications to Icelandic basalts. *Earth and Planetary Science Letters* **37,** 380–392.

Manning, C. E. (1994) The solubility of quartz in H_2O in the lower crust and upper mantle. *Geochimica et Cosmochimica Acta* **58,** 4831–4839.

Moecher, D. P., Essene, E. J. and Valley, J. W. (1992) Stable isotopic and petrological constraints on scapolitization of the Whitestone meta-anorthosite, Grenville Province, Ontario. *Journal of Metamorphic Geology* **10,** 745–762.

Newman, J. and Mitra, G. (1993) Lateral variations in mylonite zone thickness as influenced by fluid-rock interactions, Linville Fall Faults, North Carolina. *Journal of Structural Geology* **15,** 849–863.

O'Hara, K. D. (1988) Fluid flow and volume loss during mylonitization—an origin for phyillonite in an overthrust setting, North Carolina, U.S.A. *Tectonophysics* **156,** 21–36.

O'Hara, K. D. and Blackburn, W. H. (1989) Volume loss model for trace element enrichments in mylonites. *Geology* **17,** 524–527.

Passchier, C. W., Myers, J. S. and Kroner, A. (1990) *Field geology of high-grade gneiss terranes*. Springer Verlag, Berlin.

Rast, N. and Horton, J. W. Jr (1989) Melanges and olistostromes in the Appalachians of the United States and mainland Canada: an assessment. In *Melanges and Olistostromes of the U.S. Appalachians*, eds J. W. Horton Jr and N. Rast, pp. 274–269. Geological Society of America Special Paper. Geological Society of America, Boulder, Colorado, **228**.

Rollinson, H. (1989) *Using geochemical data: evaluation, presentation, interpretation*. Longman Scientific Technical, New York.

Simpson, C. and Wintsch, R. P. (1989) Evidence for deformation-induced K-feldspar replacement by myrmekite. *Journal of Metamorphic Geology* **7,** 261–275.

Sinha, A. K., Hewitt, D. A. and Rimstidt, J. D. (1986) Fluid-rock interaction and element mobility in the development of ultramylonites. *Geology* **14,** 883–886.

Sinha, A. K., Hewitt, D. A. and Rimstidt, J. D. (1986) Fluid-rock interaction and element mobility in the development of ultramylonites. Geology. *14* **,** 883–886.

Sinha, A. K., Hewitt, D. A. and Rimstidt, J. D. (1988) Metamorphic petrology and strontium isotope geochemistry associated with the development of mylonites: An example from the Brevard fault zone. *North Carolina American Journal of Sciences* **288A,** 115–147.

Taylor, S. R. and McLennan, S. M. (1985) *The continental crust: its composition and evolution*. Blackwell, Oxford.

Tucillo, M. E., Mezger, K. M., Essene, E. J. and van der Pluijm, B. A. (1992) Thermobarometry, geochronology, and the interpretation of *P–T–t* data in the Britt Domain, Ontario Grenville Orogen, Canada. *Journal of Petrology* **33,** 1225–1259.

van Breemen, O., Davidson, A., Loveridge, W. D. and Sullivan, R. W. (1986) U–Pb geochronology of Grenville tectonites, granulites and igneous precursors, Parry Sound, Ontario. In *The Grenville Province*. eds J. M. Moore, A. Davidson, A. J. Baer, pp. 191–207. Geological Association of Canada Special Paper, **31**.

White, J. C. and Mawer, C. K. (1986) Extreme ductility of feldspars from a mylonite, Parry Sound, Canada. *Journal of Structural Geology* **8,** 133–143.

Yang, X. Y., Xie, G. and Li, Z. (1995) Fluid-rock interactions and mass balance of deformed rocks during deformation. *Science in China* **25,** 329–336.

APPENDIX

In the case of two-component mechanical mixing under closed system conditions, mass balance of immobile elements gives:

$$X_A = M_{\mathrm{r}}^A/(M_{\mathrm{r}}^A + M_{\mathrm{r}}^B) \tag{A1}$$

where X_{A} is mass fraction of end-member A; $M_{\mathrm{r}}^{\mathrm{A}}$, $M_{\mathrm{r}}^{\mathrm{B}}$ are mass of end-member A and B, respectively. Thus,

$$M_{\mathrm{r}}^C = X_A M_{\mathrm{r}}^A + (1 - X_A) M_{\mathrm{r}}^B \tag{A2}$$

where M_{r}^C is the mass of rock C (mixed product); this equation can be modified to include mass transfer (ΔM) under open system conditions:

$$M_{\mathrm{r}}^C = X_A M_{\mathrm{r}}^A + (1 - X_A) M_{\mathrm{r}}^B + \Delta M \tag{A3}$$

For any immobile element i:

$$M_i^C = X_A M_i^A + (1 - X_A) M_i^B \tag{A4}$$

where M_i^A, M_i^B, M_i^C are the mass of the immobile element i in rock A, B, and C, respectively. Because:

$$M_i^C = C_i^C \times M_{\mathrm{r}}^C = C_i^C \times [X_A M_{\mathrm{r}}^A + (1 - X_A) M_{\mathrm{r}}^B + \Delta M] \tag{A5}$$

Combining equation (A4) and (A5)

$$C_i^C = 1/M_{\mathrm{r}}^C [X_A C_i^A M_{\mathrm{r}}^A + (1 - X_A) C_i^B M_{\mathrm{r}}^B] \tag{A6}$$

where C_i^A, C_i^B, and C_i^C are the concentration of the immobile element i in rock A, B, C respectively. If we mix A and B with unit mass m (such as 100 grams), equation (A6) can be simplified to:

$$C_i^C = m/(m + \Delta M)[X_A C_i^A + (1 - X_A) C_i^B] \tag{A7}$$

Under closed system conditions, $\Delta M = 0$.